Physica Medica 64 (2019) 114–122

Contents lists available at ScienceDirect

Physica Medica

journal homepage: www.elsevier.com/locate/ejmp

Original paper

Microdosimetry at the CATANA 62 MeV proton beam with a sealed miniaturized TEPC

V. Conte[a,*], A. Bianchi[a,b,c], A. Selva[a], G. Petringa[d], G.A.P. Cirrone[d], A. Parisi[b], F. Vanhavere[b], P. Colautti[a]

[a] INFN Laboratori Nazionali di Legnaro, viale dell'Università 2, 35020 Legnaro, Italy
[b] Belgian Nuclear Research Centre, SCK·CEN, Boeretang 200, 2400 Mol, Belgium
[c] UHasselt, Faculty of Engineering Technology, Centre for Environmental Sciences, Nuclear Technology Center, Agoralaan, 3590 Diepenbeek, Belgium
[d] INFN Laboratori Nazionali del Sud, via S. Sofia 62, 95123 Catania, Italy

ARTICLE INFO

Keywords:
TEPC
Microdosimetry
Proton therapy
Proton RBE

ABSTRACT

A new mini-TEPC with cylindrical sensitive volume of 0.9 mm in diameter and height, and with external diameter of 2.7 mm, has been developed to work without gas flow. With such a mini counter we have measured the physical quality of the 62 MeV therapeutic proton beam of CATANA (Catania, Italy). Measurements were performed at six precise positions along the Spread-Out Bragg Peak (SOBP): 1.4, 19.4, 24.6, 29.0, 29.7 and 30.8 mm, corresponding to positions of clinical relevance (entrance, proximal, central, and distal-edge of the SOBP) or of high lineal energy transfer (LET) increment (distal-dose drop off). Without refilling the microdosimeter with new gas, the measurements were repeated at the same positions 4 months later, in order to study the stability of the response in sealed-mode operation.

From the microdosimetric spectra the frequency-mean lineal energy $\overline{y}_F$ and the dose-mean lineal energy $\overline{y}_D$ were derived and compared with average LET values calculated by means of Geant4 simulations. The comparison points out, in particular, a good agreement between microdosimetric $\overline{y}_D$ and the total dose-average $\bar{L}ET_d$, which is the average LET of the mixed radiation field, including the contribution by nuclear reactions.

1. Introduction

Proton therapy is a fast-growing cancer treatment strategy [1]. The potential clinical advantages of proton beams are related to the pattern of energy deposition termed as the "Bragg curve", which exhibits a well-defined, highly localized peak at the end of the proton track [2]. Based on the needs of clinical application, the Bragg peak can be spread out by modulating the proton energy to attain the desired uniform dose deposition throughout the target volume.

When using particles other than photons one has to weight the physical dose with the correspondent Relative Biological Effectiveness (RBE). Indeed, the microscopic distribution of the energy deposited by a single particle, not just the total energy deposit, is very important in determining the biological effect. Low LET particles produce a few interactions in many cells. High LET particles produce clusters of interactions in fewer cells. These clusters of interactions induce clustered damages of high complexity that are difficult for the cell to repair [3,4]. The biological quality of ionizing radiation thus depends, with good approximation, on the LET of the interacting particles.

The interactions of high-energy protons with matter give rise to a complex mixed radiation field, which is populated by different particles with different LET values. At any depth, the radiation damage to living systems is due to both primary and secondary particles originating from non-elastic nuclear interactions [5]. The RBE of the mixed radiation field is then the result of several components of different RBE. Current clinical practice adopts a constant RBE value of 1.1 across the entire Spread-Out Bragg Peak (SOBP). However, radiobiological studies report RBE values increasing along the SOBP, reaching 1.3–1.4 in the distal Bragg peak and 1.7 downstream [6]. As radiobiological measurements are expensive and very time consuming, the assessment of RBE can be more conveniently based on the dose-average LET ($\bar{L}ET_d$) as a valuable physical parameter [7].

The LET can be computed with Monte Carlo (MC) models capable of transporting all the primary and secondary particles. Various techniques have been used to score LET in MC simulations. The accuracy and precision of the MC calculation results depend strongly on the physical interaction cross sections applied as well as the simulation algorithms used. Uncertainties on the cross sections, sensitivity of the LET

* Corresponding author.
E-mail address: conte@lnl.infn.it (V. Conte).

https://doi.org/10.1016/j.ejmp.2019.06.011
Received 17 April 2019; Received in revised form 13 June 2019; Accepted 23 June 2019
Available online 10 July 2019

distributions to changes in commonly adjusted simulation parameters, and calculation time for high resolution studies, are among the main limitations of MC codes. An experimental monitoring of $L\bar{E}T_d$ inside the real therapeutic beam could be a fast way to improve the RBE assessment for an optimized treatment planning.

Microdosimetry measures not just average dose but the pattern of dose deposition at the micrometric scale [8]. Over the last few decades, silicon- and diamond based microdosimeters have been developed [9–12], able to cope with high beam currents typical of proton therapy. However, the reference microdosimeter is the tissue-equivalent proportional counter (TEPC), which measures the spectrum of ionization events occurring in a gaseous volume at the passage of each single ionizing particle. The mini-TEPC developed at the Legnaro National Laboratories of the National Institute for Nuclear Physics (LNL-INFN) sustains without significant pile-up fluence-rates higher than those sustained by the smallest commercial proportional counter, i.e. the LET1/2 counter manufactured and sold by Far West Technology, Inc.© [13]. Moreover, thanks to overall dimensions of only a few millimetres, it allows high spatial resolution, both in the direction of the particle beam and transversally. Unfortunately, this mini-TEPC required a continuous gas flow, to assure a good stability of the gas gain. The encumbrance of the overall experimental setup, including an ancillary gas flowing equipment, and the considerable care required for the mini-TEPC handling and the associated data logging and analysis has hampered its widespread use so far. In order to facilitate the use of microdosimetry in clinical environment, this work presents a new version of the mini-TEPC developed at LNL, which can work without continuous gas flow. The performances of this device were tested at the 62 MeV proton SOBP of CATANA, and microdosimetric quantities were compared with mean LET values obtained by Monte Carlo Geant4 simulations.

2. Material and methods

2.1. The microdosimeter

The new mini-TEPC developed at LNL copies the one that had already measured in therapeutic proton [14,15] and carbon radiation fields [16,17]. The gas and vacuum ducts have been modified to improve the counter cleaning from plastic degassing as well as washing and gas filling procedures. Apart from that, the new mini-TEPC has the same design as the previous TEPC published earlier in [14–17]. It has a cylindrical sensitive volume 0.9 mm in diameter and height, surrounded by a 0.35 mm-thick A-150-cathode wall, a 0.35 mm Rexolite® insulator, a 0.2 mm-thick titanium sleeve for a total external diameter of 2.7 mm. The sensor stands inside the 150 mm long titanium sleeve. The PMMA-equivalent wall thickness of the detector is 1.18 mm, as it results by taking into account the average stopping-power ratio of protons within the different materials. A drawing of the mini-TEPC is given in Fig. 1.

This modified mini-TEPC operates in gas-steady modality, instead of being continuously fluxed with new gas.

The detector was cleaned by high vacuum pumping for a few days followed by a continuous gas flow with pure propane-gas for an additional few days. Afterwards, it was filled with propane at a pressure of 45.4 kPa at 21.8 °C, the inlet valve was then closed for operating the detector without gas refilling.

The pressure was monitored via an absolute Baratron® capacitance manometer connected to the detector. During the 4-months period between the two measurement campaigns, the gas pressure variation was less than 3%.

At the pressure of 45.4 kPa the sensitive volume mass thickness is 0.075 mg/cm^2, which is equivalent, in terms of mean imparted energy, to 0.85 μm of liquid water, by taking into account the mean ratio of the mass-stopping powers of protons in propane and water, calculated with SRIM [18].

2.2. Experimental set-up and data processing

Measurements were performed at the CATANA proton therapy centre of the Southern National Laboratories of INFN in Catania (LNS-INFN). The 62 MeV modulated proton beam penetration range, measured at the distal 80% dose level of the Bragg peak (R80), was 2.95 cm in water; the modulation width was 1.1 cm. The passive energy modulation was produced with the same modulator wheel that is daily used in clinical practice. The sensitive volume of the mini-TEPC was aligned with the centre of the proton beam, the diameter of which was 25 mm.

Measurements were performed at 6 precise positions along the Spread-Out Bragg Peak: 1.4, 19.4, 24.6, 29.0, 29.7 and 30.8 mm in water-equivalent depths, corresponding to positions of clinical relevance (entrance, proximal, central, and distal end of the SOBP) or of high LET increment (distal-dose fall off). A statistics of at least 10^6 events was acquired at each position, for a delivered dose to the sensitive volume of about 0.2 Gy at the entrance (1.4 mm) and about 3 Gy at the distal fall-off (30.8 mm). The depth was determined by placing a stack of PMMA layers of different thickness between the counter and the beam collimator. The effective depth was calculated by adding the 1.18 mm PMMA-equivalent thickness of the detector. The equivalent depth in water was calculated by multiplying the PMMA depth by a factor 1.16, which takes into account the mean ratio of the total linear stopping power of protons in PMMA and in water, calculated with SRIM [18]. The uncertainty on the water depth was evaluated as 0.15 mm. Fig. 2 shows a picture of the experimental set-up at the CATANA proton therapy centre, with the detector positioned at the isocenter.

Without refilling the microdosimeter with new gas, the measurements were repeated at the same positions 4 months later, in order to study the stability of the detector response in sealed-mode operation.

All the measurements were performed with the anode wire grounded through the preamplifier and the cathode wall biased at −700 V. The gas gain was enough to collect events down to 0.4 keV/μm of size (about 12 ionisations). Three spectroscopy linear amplifiers of different gains were used to shape and amplify simultaneously pulses from the preamplifier. The amplifier shaping times were set at 500 ns, and the beam current was adjusted to maintain a constant 10 kHz counting rate at the detector. The beam current was reduced to 50 pA, as compared to the clinical value of about 5nA. No pile up effects were observed during irradiations. A precision research pulser was used to calibrate the three electronic chains. Individual pulses from the preamplifier were fed into a NIM/CAMAC/PC based data acquisition system for analogue and digital signal processing. The three sub-spectra were joined off-line by superimposing the common parts.

The spectrum energy calibration was performed by making use of the proton-edge, which is clearly visible at the depth 30.8 mm and corresponds to the maximum energy that protons can release in the sensitive volume. The proton edge region in the $yd(y)$ spectrum was fitted by a Fermi-fit function, and the position of the inflection point of the fitted function was determined as the proton-edge position with a precision of 3%, following the method described by Conte V. et al. [19]. According to SRIM [18], the maximum stopping power of protons in propane-gas results in a maximum lineal energy value of 162 keV/μm. Multiplied by the mean mass stopping-power ratio $S_m^{(water)}/S_m^{(propane)}$ this gives a *y*flex value of 143 keV/μm that was assigned to the position of the inflection point. The same calibration factor was then used to calibrate also the other spectra. The frequency spectra $f(y)$ were linearly fitted between 0.4 and 0.5 keV/μm and extrapolated down to 0.01 keV/μm and then processed to obtain the $yd(y)$ against the log(y) distribution and the $\bar{y}_D$ value.

The frequency-mean lineal energy and the dose-mean lineal energy values have been calculated according to the following equations:

$$\bar{y}_F = \int y f(y) dy \quad (1)$$

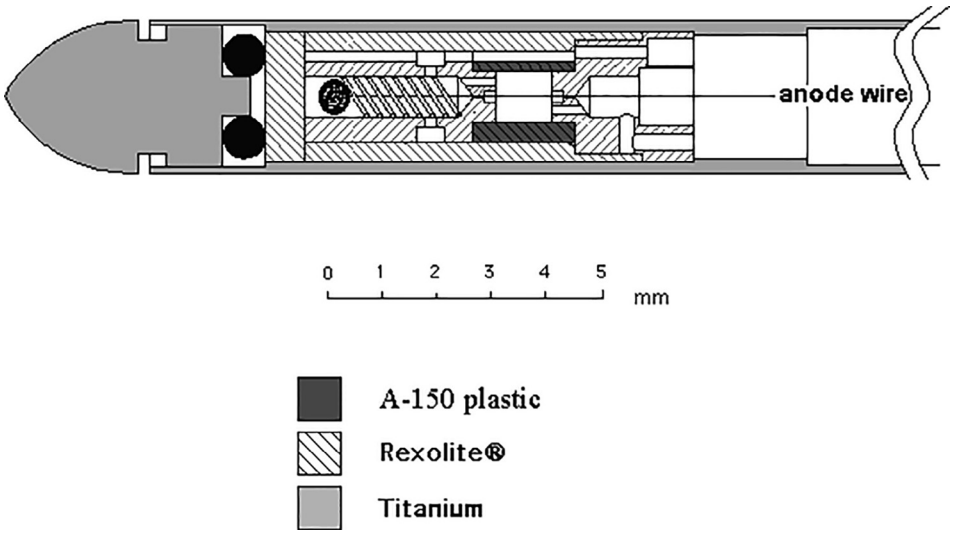

Fig. 1. A cross-section drawing of the mini-TEPC.

$$\overline{y}_D = \frac{\int y^2 f(y)dy}{\int yf(y)dy} \quad (2)$$

The saturation corrected dose mean lineal energy y^* was also calculated, because it is used to assess the biological effectiveness of particle beams in the modified MKM model [20]. The following equation was used, with the saturation value $y_0 = 124\,\text{keV}/\mu\text{m}$, as first suggested by Kellerer [21] and then recommended also in the ICRU Report 36 [22]:

$$y^* = y_0^2 \frac{\int \left(1 - \exp\left(-\frac{y^2}{y_0^2}\right)\right) f(y)dy}{\int yf(y)dy} \quad (3)$$

Alternatively to the MKM model, microdosimetric lineal energy spectra can be used to estimate the RBE by using a suitable weighting function $r(y)$ according to the following equation:

$$\text{micro} - RBE = \int r(y)d(y)\text{dy} \quad (4)$$

where $d(y)$ is the measured dose distribution of the lineal energy y. The acronym "*micro-RBE*" wants to underline the difference from the radiobiological data. In this work we have used the weighting function published by Loncol et al. [23].

3. Dose and dose-average let calculations

The CATANA transport beamline is simulated with HADRONTHERAPY [24], a free and open source application currently available inside the public release of the Geant4 [25] Monte Carlo code. A completely new module, with respect to that reported in [26], was recently implemented inside the application. It allows to study the LET distributions in configurations that are of interest for radiobiology experiments. New developed algorithms were introduced to produce results independent from the simulation transport parameters such as voxel size, secondary particle threshold (production cuts) and step length [27]. The module was used in this work to calculate the track-average LET ($\bar{\text{LET}}_t$), and the dose-average LET ($\bar{\text{LET}}_d$), of the specific modulated

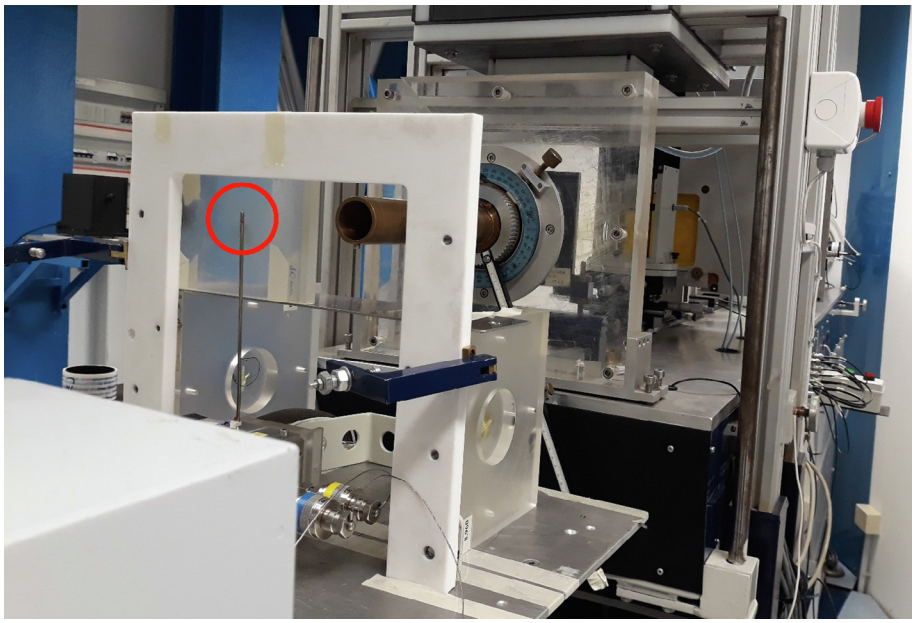

Fig. 2. A picture of the experimental set-up with the mini-TEPC (highlighted by a red circle) positioned at the isocenter. (For interpretation of the references to colour in this figure legend, the reader is referred to the web version of this article.)

Bragg peak used. To calculate $L\bar{E}T_t$ and $L\bar{E}T_d$ at a given water depth, the track- and the dose-average LET values of each particle were weighted with their relative frequency and dose contribution, respectively. The following equations were used:

$$L\bar{E}T_t(z) = \frac{\sum_{j=1}^{n} \int_0^{\infty} S_{el}^{j}(E)\varphi_E^j(z)dE}{\sum_{j=1}^{n} \varphi_E^j(z)dE} \quad (5)$$

$$L\bar{E}T_d(z) = \frac{\sum_{j=1}^{n} \int_0^{\infty} S_{el}^{j^2}(E)\varphi_E^j(z)dE}{\sum_{j=1}^{n} \int_0^{\infty} S_{el}^{j}(E)\varphi_E^j(z)dE} \quad (6)$$

where $L\bar{E}T_d(z)$ is the $L\bar{E}T_d$ at the depth z in the water phantom, S_{el}^j is the electronic stopping power of the particle j of energy E and $\varphi_E^j(z)$ is the number of particles of type j that have energy E at depth z. The integral is performed over the entire energy range of the particle j and the sum is done over all charged particles set in motion by the protons.

In particular, this new tool allows to compute the dose-average LET considering in the computation both primary and secondary particles originating from non-elastic nuclear interactions. In that case the dose-average LET is indicated as total-$L\bar{E}T_d$, otherwise as primary-$L\bar{E}T_d$.

The simulated relative absorbed dose, the primary and the total-$L\bar{E}T_d$ are plotted against the water depth in Fig. 3. Measurements performed with the Markus chamber are also shown. The vertical dashed lines indicate the water-equivalent positions of the microdosimetric measurements.

A non-negligible difference emerges in the $L\bar{E}T_d$ in the entrance channel, whether the secondary contribution is taken into account or not. Indeed, the total-$L\bar{E}T_d$ is about three times higher than the primary-$L\bar{E}T_D$, when only primary incident protons are considered. The $L\bar{E}T_d$ curves show an almost-constant behaviour up to 18 mm in depth, with values < 5 keV/μm typical of low LET radiations. Then, they increase slowly up to 28 mm, in correspondence with the uniform-dose region of the SOBP, and finally they increase sharply in the distal and fall-off regions, between 28 and 31 mm, as already observed in [28].

At the last position, corresponding to a depth of 30.8 mm in water and indicated as P6 in Fig. 3, the dose level is only 0.4% of the maximum but the total-$L\bar{E}T_d$ increases from about 5 keV/μm at the entrance to more than 30 keV/μm.

The relative-dose and the average-LET values are listed in Table 1, for the six specific positions at which microdosimetric measurements were performed.

On the other hand, the total-$L\bar{E}T_t$, calculated including also secondary particles, was the same as the primary-$L\bar{E}T_t$ within statistical

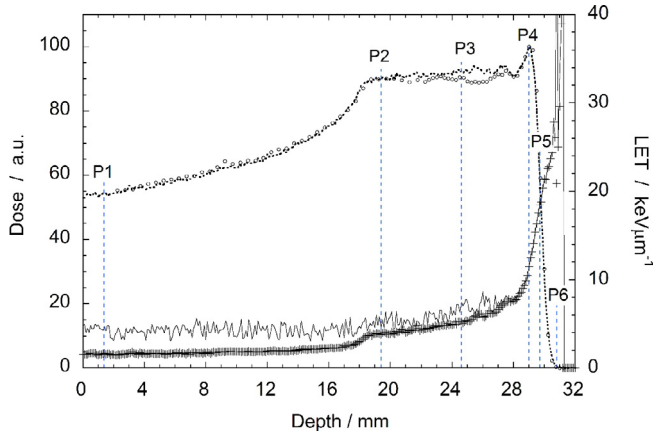

Fig. 3. MC simulations: relative-dose (dotted line), primary $L\bar{E}T_d$computed for only primary protons (crosses) and total $L\bar{E}T_d$, considering also the contribution of generated secondary particles (thin solid line). Calculations performed in water with HADRONTHERAPY-Geant4 simulations. Circles are the dose-values measured with the Markus Chamber. Vertical dashed vertical lines indicate the positions at which microdosimetric measurements were performed.

Table 1
MC simulations: relative-dose and average-LET values at the six specific positions at which microdosimetric measurements were performed. Positions are given in terms of water equivalent thickness.

Position mm	Relative dose a.u.	Primary $L\bar{E}T_t$ keV μm^{-1}	Primary $L\bar{E}T_d$ keV μm^{-1}	Total $L\bar{E}T_d$ keV μm^{-1}
1.4	54.2	1.28	1.64	4.45
19.4	89.9	2.43	3.79	5.06
24.6	92.4	3.34	5.29	7.07
29.0	100	7.87	11.5	11.5
29.7	60.5	12.3	18.5	18.4
30.8	0.40	18.2	20.9	32.7

uncertainties, possibly due to the fact that the relative contribution of the secondary particles to the total fluence is small, of the order of 10^{-4} (see later discussion on Fig. 7).

More details about Monte Carlo model and the used algorithms are given in References [24,26,27].

4. Experimental results and discussion

4.1. Microdosimetric spectra

Microdosimetric measurements were performed at 6 different depths along the SOBP, indicated in Fig. 3 as P1, P2, P3, P4, P5, P6, and repeated in the same experimental conditions about 4 months later. The comparison of the microdosimetric spectra collected at different times is shown in Fig. 4, for each measuring position from P1 to P6. The good agreement between the paired distributions is clearly visible, indicating a good stability of the detector response in the steady-gas modality without gas refilling.

To give an impression of how the lineal energy spectrum changes with increasing depth along the SOBP, a set of six measured spectra is shown together in Fig. 5.

At 1.4 mm of depth (position P1 in Fig. 3), the majority of absorbed dose is delivered by events of size about 1 keV/μm, which correspond to stopping power values of 60 MeV protons. However, a fraction of the dose is released by events ranging from 20 to several hundreds of keV/μm, as already observed in previous microdosimetric measurements performed at the proton therapy centre Antoine Lacassagne of Nice [14]. These events are due to secondary particles produced in nuclear interactions by fast protons in the entrance channel. Even if these events have a low probability of occurrence (about 0.015%) they contribute with 1.2% to the dose, because they are relatively high LET events.

Moving along the SOBP toward the Bragg peak, the protons slow down and the spectra shift correspondingly to higher y values, as it can be seen in Fig. 5. At the Bragg peak, the majority of the dose is due to events around 7 keV/μm, due to protons of about 5.5 MeV energy and 0.5 mm residual range. Downstream the Bragg peak the maxima of the spectra move further to higher y values, corresponding to slowed-down protons of increased LET; the proton edge, corresponding to the maximum energy that protons can release in the simulated water-site, is clearly visible. This component is due to low-energy protons of about 100 keV of energy.

The mean values of frequency and dose distributions of the lineal energy can be calculated according to Eqs. (1)–(3) (with a saturation level y_0 = 124 keV/μm). As a consequence of the good agreement between the paired spectral distributions, the derived average quantities $\bar{y}_F$, $\bar{y}_D$ and y^* are also consistent. The values obtained in the two different measurement campaigns are listed in Table 2 and plotted in Fig. 6. The paired mean values are always in good agreement, in particular the $\bar{y}_D$ values differ by less than 3%. Based on these measurements, the type-A relative standard uncertainties on $\bar{y}_F$, $\bar{y}_D$ and y^*, according to GUM definitions [29], were estimated as 7%, 5% and 5%

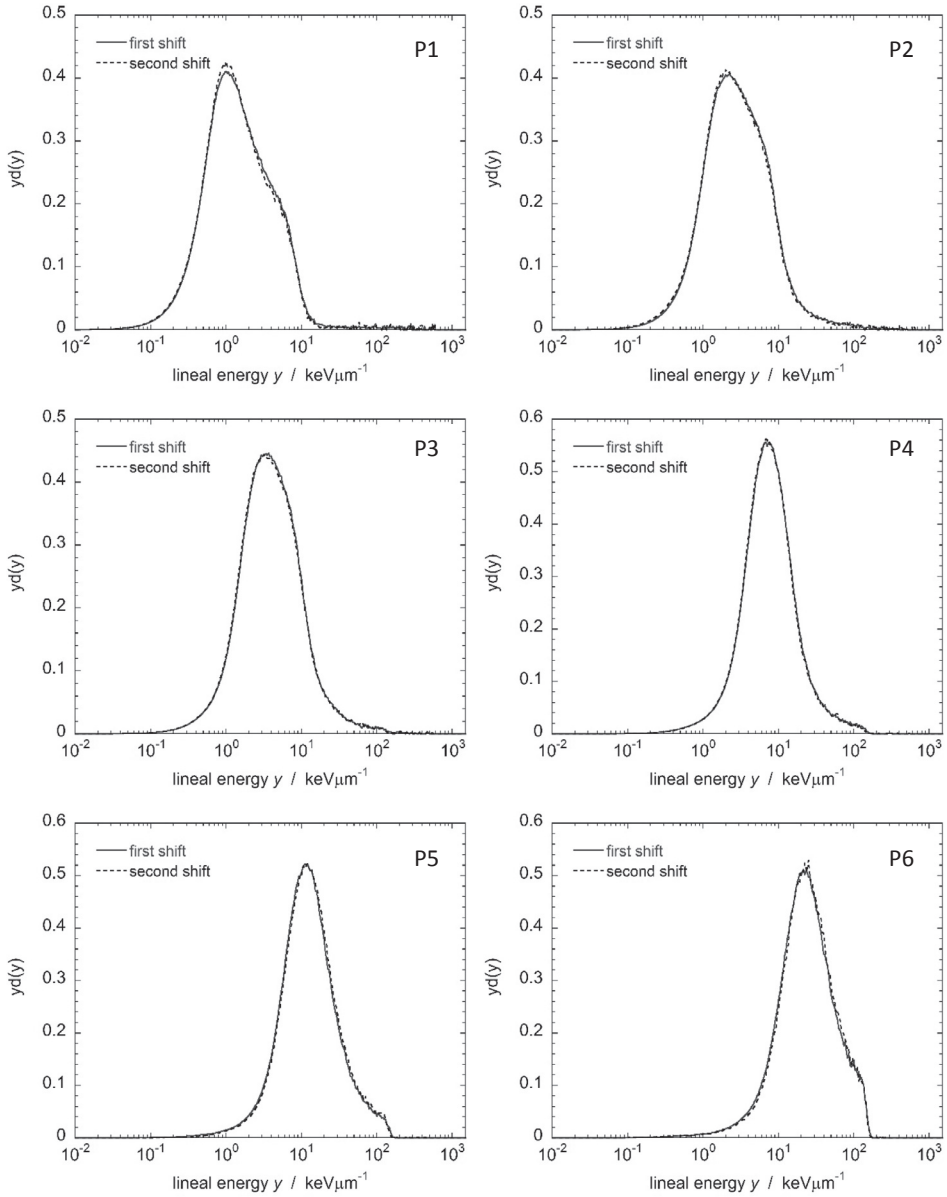

Fig. 4. Paired microdosimetric distributions, measured approximately 4 months apart, at 6 precise depths along the SOBP, P1 = 1.4 mm, P2 = 19.4 mm, P3 = 24.6 mm, P4 = 29.0 mm, P5 = 29.7 mm, P6 = 30.8 mm.

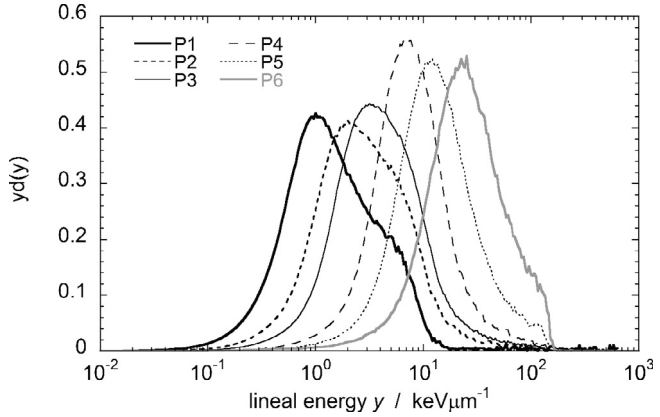

Fig. 5. The first set of $yd(y)$ microdosimetric distributions measured at six different positions along the SOBP.

respectively.

To give an impression of the influence of events with lineal energy above a given threshold level, likely originating from non-elastic nuclear interactions, left side of Fig. 7 shows the $yd(y)$ spectrum measured in the entrance channel (depth = 1.4 mm) together with 1-$F(y)$ and 1-$D(y)$, representing respectively the complementary cumulative frequency- and dose- distribution functions, i.e. the fraction of events and the fraction of dose corresponding to events greater or equal to y. High LET events, though rare (about 10^{-4} cumulative probability of occurrence), deposit significant dose contributions (about 1% of the dose).

Right side of Fig. 7 shows, together with $yd(y)$, the frequency mean lineal energy ($\bar{y}_F$,) and the dose mean lineal energy ($\bar{y}_D$), as a function of the lineal energy y as upper cut-off in the integrations of Eqs. (1) and (2). It is clearly visible that events with y > 20 keV/μm (the value 20 keV/μm is highlighted by vertical dashed lines) give almost no contribution to $\bar{y}_F$, due the low occurrence probability, whereas $\bar{y}_D$ increases from about 2 to about 4 keV/μm, in good consistency with the difference between calculated primary and total $\bar{LET}_d$ (1.64 and 4.45 keV/μm respectively, according to data listed in Table 1). It is

Table 2
The values obtained in the two different measurement campaigns.

Position mm	$\bar{y}_F$-shift 1 keV μm–^{1}	$\bar{y}_F$-shift 2 keV μm^{-1}	$\bar{y}_D$-shift 1 keV μm^{-1}	$\bar{y}_D$-shift 2 keV μm^{-1}	y^*-shift 1 keV μm^{-1}	y^*-shift 2 keV μm^{-1}
1.4	0.85	0.82	3.58	3.87	2.81	2.74
19.4	1.65	1.57	5.57	5.66	4.92	4.74
24.6	2.21	2.34	6.64	6.91	5.96	6.25
29.0	4.84	4.86	11.1	10.9	10.5	10.4
29.7	7.24	8.08	18.3	18.9	16.8	17.4
30.8	14.5	15.7	32.4	33.2	28.4	29.1

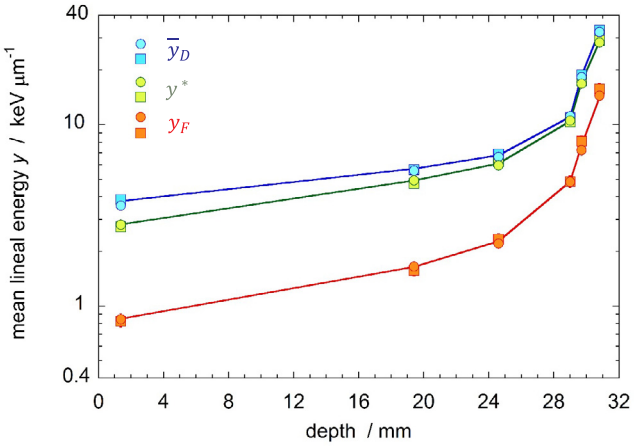

Fig. 6. Measured $\bar{y}_F$, $\bar{y}_D$ and y^* as a function of water-depth. Circles refer to the first measurements set, squares are the measurements performed 4 months later. Error bars representing the estimated uncertainties (7% on $\bar{y}_F$, 5% on $\bar{y}_D$ and y^*) fall within symbols. Lines connect the mean values of paired data.

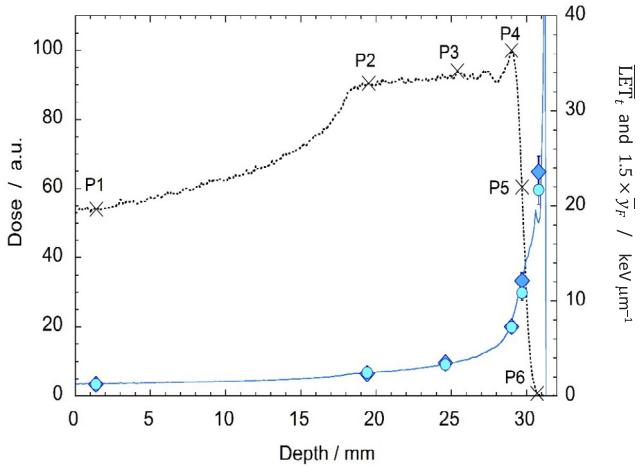

Fig. 8. Relative dose (dotted-line) and track-average $\bar{L}ET_t$(blue line) computed by MC calculations. Times symbols indicate the positions of measurements. Circles and diamonds are the $1.5 \times \bar{y}_F$ values, as a function of depth in water. Circles refer to the first measurements, diamonds to measurements performed in the same experimental conditions (4) months later. Vertical error bars represent the type-A standard uncertainties (see text). Horizontal error bars (0.15 mm) are within symbols.

therefore important to acquire a statistic of at least 10^6 events, to reduce statistical fluctuations of rare events that, due to their high LET, contribute significantly to the dose-mean lineal energy.

4.2. Mean lineal energy and calculated let values

The frequency-mean lineal energy $\bar{y}_F$ has been compared to the simulated track-average $\bar{L}ET_t$. It turned out that $\bar{y}_F$ has a similar trend with depth as the $\bar{L}ET_t$, but it is always lower of about 30% along the whole SOBP. When multiplied by a factor 1.5, the experimental $\bar{y}_F$ values reproduce the calculated track-average $\bar{L}ET_t$ very satisfactorily, as shown in Fig. 8. The reason for this factor needs further investigation; it is possibly due to an overestimation, in the lineal energy spectra, of the component of small energy deposits related to the chord length distribution of the cylindrical sensitive volume. The type-A relative standard uncertainty on $\bar{y}_F$ (7%), is consistent with the propagation of uncertainties related to the lineal energy calibration [17,19], the linear extrapolation to 0.01 keV/μm and the statistical fluctuations.

From the dose-distributions of lineal energy, the $d(y)$ spectra, the dose-mean lineal energy was also calculated, according to Eq. (2). Fig. 9 shows the measured dose-mean lineal energy $\bar{y}_D$ together with the primary-$\bar{L}ET_d$ and the total-$\bar{L}ET_d$. The $\bar{y}_D$values are almost the same as the total-$\bar{L}ET_d$. The differences with the primary $\bar{L}ET_d$ are significant in the entrance channel, where the contribution of secondary particles produced in non-elastic nuclear interactions plays a larger role. This

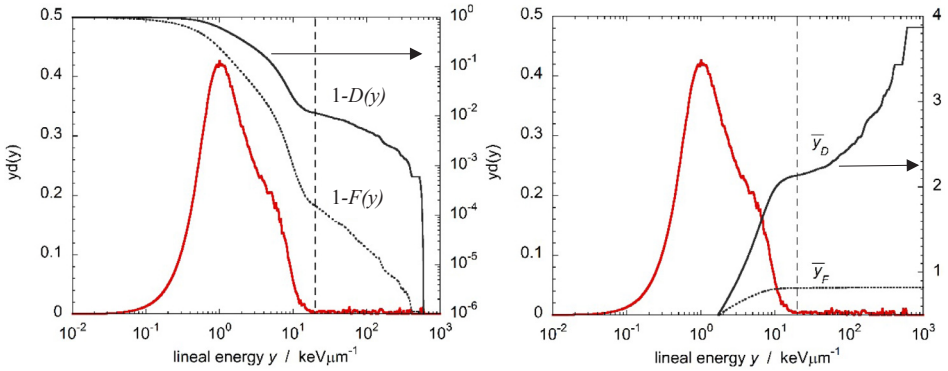

Fig. 7. Microdosimetric spectrum at 1.4 mm of water-equivalent depth. In the left figure, the cumulative fraction of events > y and the corresponding cumulative fraction of dose are also plotted. The right figure shows the variation of $\bar{y}_D$ and $\bar{y}_F$ as a function of y as the upper limit of the integration to calculate the mean values. Vertical dashed lines point out the 20 keV/μm value of y.

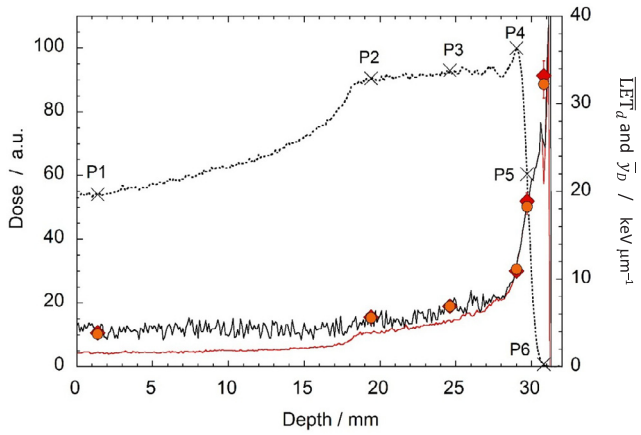

Fig. 9. Relative dose (dotted line) and $\bar{y}_D$ values against the depth in the water phantom. Circles refer to the first measurements, diamonds to measurements performed in the same experimental conditions (4) months later. Depth uncertainty is 0.15 mm (within symbols) and $\bar{y}_D$ uncertainty is 5%. The black line is the total $L\bar{E}T_d$, the red line is the primary $L\bar{E}T_d$ (see Section 3).

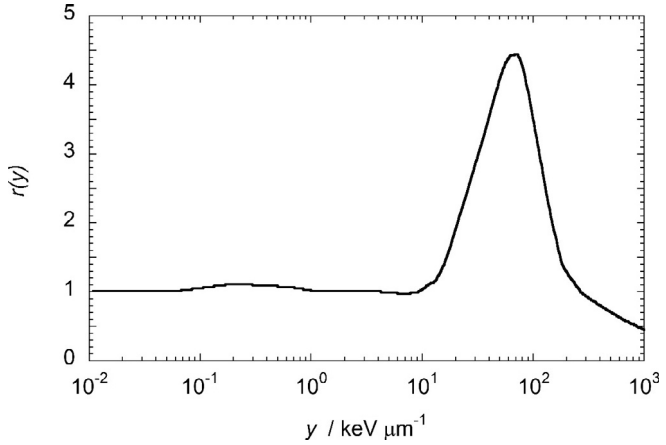

Fig. 11. Biological weighting functions $r(y)$ for early intestinal tolerance assessed by crypt regeneration in mice (single fraction with 8 Gy) as the biological end point. Redrawn after Loncol et al. [23].

good agreement suggests that the dose-mean lineal-energy $\bar{y}_D$, measured with a sealed mini-TEPC, can model the total-$L\bar{E}T_d$ of a 62 MeV proton-modulated Bragg peak, along the whole SOBP.

The direct relationship between $\bar{y}_D$ and total-$L\bar{E}T_d$ is shown in Fig. 10, where the total-$L\bar{E}T_d$ values were calculated at the specific measurement depths. Within the estimated 5% uncertainties, the measured $\bar{y}_D$ is always equal to the calculated total-$L\bar{E}T_d$.

Differences in the calculated total-$L\bar{E}T_d$ values resulting from a depth uncertainty of 0.15 mm are also plotted as error bars on the x-axis. In the distal region a shift of 0.15 mm in the backward or in the forward direction leads to significant changes in the calculated total-$L\bar{E}T_d$, because in this region the $L\bar{E}T_d$ varies very quickly, with first a steep increment and finally a sharp drop-off, as it can be seen in Fig. 9.

4.3. The mini-tepc as a radiation quality monitor

Once that a detector is available for measuring the microscopic lineal energy distributions at various depths inside a phantom, the question arises how to link measured physical quantities to the biological quality of the radiation field. There are basically two approaches that allow using microdosimetry to assess the RBE of clinical beams: one is the use of a biological weighting function (BWF) [6,30], the other one is the MKM model. They both have limits and potentialities. The

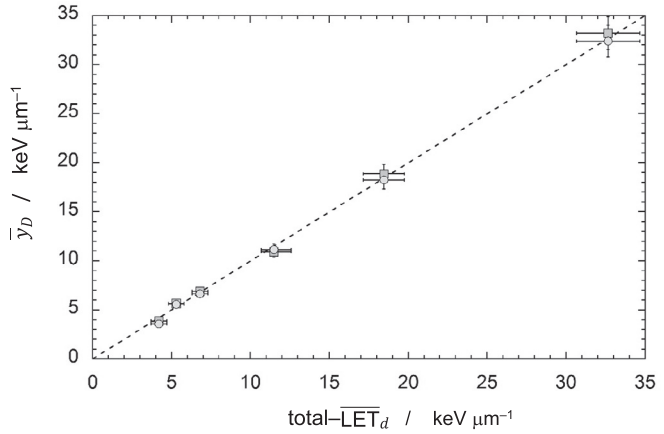

Fig. 10. Measured $\bar{y}_D$ as a function of the total $L\bar{E}T_d$. The dashed-line points out the equality between the two variables. Vertical error bars represent the 5% estimated uncertainties on $\bar{y}_D$ and horizontal bars represent the $L\bar{E}T_d$ estimated uncertainties resulting from the depth uncertainty of 0.15 mm (see text).

MKM is based on estimation of specific energy (z) in small domains. When using measured microdosimetric values for the mean specific energy, the model relies on 2 additional parameters associated to the specific cell lines. The BWF is the older approach: by using a phenomenological weighting function derived for a specific biological endpoint, the methodology allows to use microdosimetric spectra for the intercomparison of the radiation quality (in terms of assessed RBE) of different treatment centres.

The main assumption in the model is that a dose-biological effect relationship can be expressed as an integral of two separate functions of the stochastic variable y describing energy deposition events: $d(y)$, representing the dose-distribution of y in the target; and $r(y)$, representing the corresponding cellular response function. The most used biological weighting function, compiled by Loncol et al. [23], is shown in Fig. 11. It was determined in a phenomenological approach by applying unfolding calculations to different sets of RBE-$d(y)$ data pairs combining high energy gamma rays, protons and neutrons experiments with mice. The early intestinal tolerance assessed by crypt regeneration in mice was set as biological endpoint. The effect was measured after a single fraction with 8 Gy.

In order to test the capability of different models to predict specific biological outcomes, specific weighting functions are needed. However, in clinical practice, it is not obvious what biological model (cell line, in-vitro, in-vivo …) to prefer. The relevance of various reported endpoints to define clinical RBE values for tumour-control probability and for normal-tissue complication probability is still unclear. The RBE values are largely scattered when considering different end points, but it should be considered that the target medium inside the patient (cancerous and healthy tissue) is made of different asynchronous cells, with different radiosensitivity, and finally different response. Moreover, variability in radiosensitivity among different patients could be similar or even larger than general RBE variations for different end points. As a consequence of this large variability, in clinics, in order to assess the effective-dose and to optimize the therapeutic plan, it is reasonable to consider a general RBE, obtained by averaging the RBE for a variety of end-points [6,7]. For a practical estimation of the biological-quality of the radiation field, we propose to use the weighting function for early intestinal tolerance as a good, reliable and low-variance experimental test. The measured dose-weighted lineal energy distribution $d(y)$ can be used to estimate the relative biological effectiveness (RBE) of the radiation field using Eq. (4). Intestinal crypt regeneration in mice is the test of choice in performing intercomparisons between centres applying different types of non-conventional radiation qualities. It was proven to be reproducible, reliable and accurate, and becomes progressively recognized worldwide as part of the Quality Assurance (QA) procedures

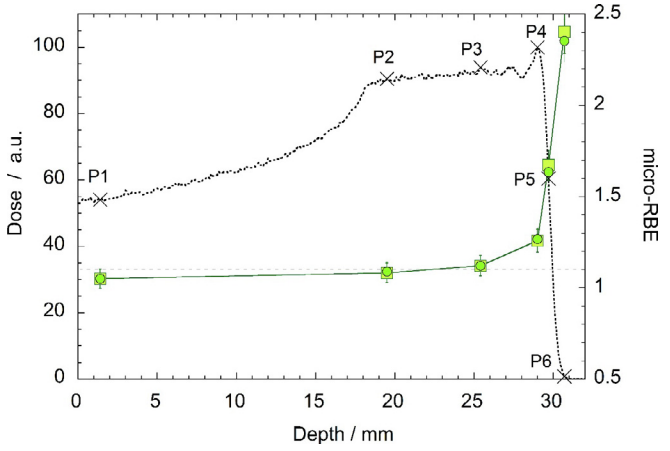

Fig. 12. The RBE estimated from $d(y)$ distributions by using the biological weighting function $r(y)$ shown in Fig. 11, according to Eq. (4). Circles are the result from the first set of microdosimetric measurements, squares refer to the measurements performed 4 months later. Error bars represent the 5% estimated uncertainty on $d(y)$. Uncertainty on the $r(y)$ weighting function is not taken into account.

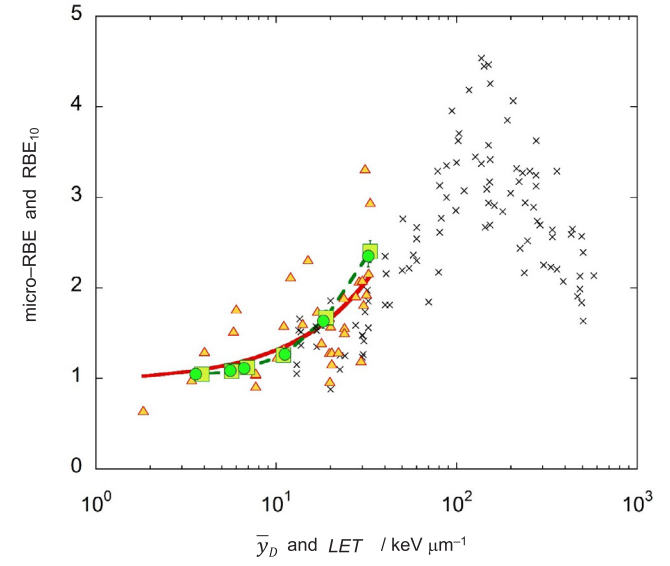

Fig. 13. Microdosimetric RBE (squares and circles) versus measured $\bar{y}_D$ and biological RBE at 10% survival for asynchronous radio-resistant cells from in vitro-experiments with monoenergetic proton (triangles) and carbon-ion (times symbols) beams [32], as a function of LET. The thick-full line is the linear fit of proton-data. Vertical bars on micro-RBE represent the 5% estimated uncertainties (only the uncertainty on $\bar{y}_D$ was taken into account).

for new beams [31].

Fig. 12 shows the micro-RBE values calculated by weighting the measured $d(y)$ spectra with $r(y)$ of Fig. 11.

In the first three positions, the micro-RBE value is approximately 1.1, it increases to 1.2–1.3 in the very distal edge and reaches a value of about 2.4 downstream. In contrast with the current clinical practice that adopts a constant RBE value of 1.1 across the entire SOBP, these values are in good accordance with several radiobiological studies [6].

Our microdosimetric estimation of the RBE was then compared with RBE10 for a variety of radio-resistant and asynchronous cell-lines irradiated by monoenergetic protons, using the data available in the PIDE library [32]. Fig. 13 shows the result of this comparison. RBE for monoenergetic carbon ions are also shown in the Figure, to show the general RBE trend with LET. The thick red line is the linear best fit of biological data for proton beams. The microdosimetric estimation of RBE (squares and circles) are plotted as a function of the measured $\bar{y}_D$, as representative of the average LET of the radiation field. It is impressive that, when compared to different biological end-points, the BWF model still leads to reasonable results without adjusting any parameter.

The microdosimetric estimation of RBE by means of the MKM model optimized to specific cell lines irradiated at the 62 MeV proton SOBP of CATANA will be the subject of a future study.

5. Conclusions

A new mini-TEPC has been constructed at the Legnaro National Laboratories to operate in sealed modality, without continuous gas flow. In order to test the reproducibility of microdosimetric measurements of the new detector, measurements were performed at 6 relevant positions of the modulated 62 MeV proton beam of CATANA, at the INFN National Laboratory of Catania, and repeated 4 months later without gas refilling of the detector. Both the gas gain and the measured spectral distribution of lineal energy were the same within statistical uncertainty. The stability of the detector was confirmed after an overall exposure of approximately 0.5 kGy to the target volume.

All the spectra were processed to calculate $\bar{y}_F$, $\bar{y}_D$ and y^*. The mean lineal energy values were the same, within estimated uncertainties. In particular, the $\bar{y}_D$-values measured 4 months apart differ by less than 3% from each other, and also from the total $\bar{L}ET_d$ calculated with the application HADRONTHERAPY of Geant4. The frequency mean lineal energy $\bar{y}_D$ was found to be proportional to the track-average $\bar{L}ET_t$, the factor of proportionality being 1.5.

The microdosimetric RBE obtained by weighting the $d(y)$ spectra with a general biological weighting function $r(y)$ are consistent with radiobiological data from in to vitro measurements available in literature. This result confirm the assumption of a correlation between the measurable microdosimetric quantities and the biological effectiveness of a proton spread out Bragg peak.

The microdosimetric approach has the advantage that $d(y)$ spectra can be easily measured in a short time. The new mini-TEPC can work in sealed mode, at fluence rates of at least 10^6 particles/s/cm$^{2.}$ This new mini-TEPC can therefore provide a practicable solution to the existing and unsolved problem of accounting for radiation quality variations in proton therapy.

Acknowledgements

This work was supported by the Italian Institute for Nuclear Physics (INFN). The Belgian nuclear research centre SCK·CEN and Hasselt University provide a Phd scholarship.

References

[1] PTCOG 2017. Hadrontherapy facilities worldwide in operation. www.ptcog.ch, (updated in January 2017).
[2] Raju MR, Amols HI, Bain E, Carpenter SG, Cox RA, et al. A heavy particle comparative study. Part III. OER and RBE. Br J Radiol 1978;51:712–9.
[3] Ward JF. Biochemistry of DNA Lesions. Radiat Res, Suppl 1985;8(104):S-103–11.
[4] Goodhead DT. Initial events in the cellular effects of ionizing radiations: clustered damage in DNA. Int J Radiat Biol 1994;65:7–17.
[5] Paganetti H. Nuclear interactions in proton therapy: dose and relative biological effect distributions originating from primary and secondary particles. Phys Med Biol 2002;47(5):747–64.
[6] Paganetti H. Relative Biological Effectiveness (RBE) values for proton beam therapy. Variations as a function of biological endpoint, dose, and linear energy transfer. Phys Med Biol 2014;59(22):R419–72.
[7] Singers Sørensen B, Overgaard J, Bassler N. In vitro RBE-LET dependence for multiple particle types. Acta Oncologica 2011;50:757–62.
[8] Rossi HH, Zaider M. Microdosimetry and its Applications p. 21 Berlin Heidelberg, New York: Springer; 1996.
[9] Agosteo S, Colautti P, Fazzi A, Moro D, Pola A. A solid state microdosimeter based on a monolithic silicon telescope. Radiat Prot Dosimetry 2006;122(1–4):382–6.
[10] Rosenfeld AB. Novel detectors for silicon based microdosimetry, their concepts and applications. Nucl Instr Meth A 2016;809:156–70.
[11] Guardiola C, Fleta C, Rodríguez J, Lozano M, Gómez F. Preliminary

microdosimetric measurements with ultra-thin 3D silicon detectors of a 62 MeV proton beam. JINST 2015;10:P01008.
[12] Verona C, Magrin G, Solevi P, Bandorf M, Marinelli M, Stock M, Verona Rinati G. Toward the use of single crystal diamond based detector for ion-beam therapy microdosimetry. Rad Meas 2018;110:25–31.
[13] De Nardo L, Cesari V, Donà G, Magrin G, Colautti P, et al. Mini-TEPCs for radiation therapy. Rad Prot Dos 2004;108:345–52.
[14] De Nardo L, Cesari V, Iborra N, Conte V, Colautti P, et al. Microdosimetric assessment of Nice therapeutic proton beam biological quality. Phys Med 2004;20(2):71–7.
[15] De Nardo L, Moro D, Colautti P, Conte V, Tornielli G, et al. Microdosimetric investigation at the therapeutic proton beam facility of CATANA. Rad Prot Dosim 2004;110(1–4):681–6.
[16] Colautti P, Conte V, Selva A, Chiriotti S, Pola A, et al. Microdosimetric study at the CNAO active-scanning carbon-ion beam. Rad Prot Dosim 2018;180(1–4):167–71.
[17] Colautti P, Conte V, Selva A, Chiriotti S, Pola A, et al. Miniaturized microdosimetrs as LET monitors: First comparison of calculated and experimental data performed at the 62 MeV/u ^{12}C beam of INFN_LNS with four different detectors. Phys Med 2018;52:113–21.
[18] Ziegler JF, Ziegler MD, Biersack JP. SRIM The stopping and range of ions in matter. Nucl Instr Meth B 2010;268:1818–23.
[19] Conte V, Moro D, Grosswendt B, Colautti P. Linear energy calibration of mini tissue equivalent gas-proportional counters (TEPC). Multidisciplinary Applications of Nuclear Physics with Ion Beams (ION BEAMS '12) – AIP Conf Proc, vol. 530. 2013. p. 171–8.
[20] Kase Y, Kanai T, Skama M, Tameshige Y, Himkai T, et al. Microdosimetric approach to NIRS-defined biological dose measurements for carbon-ion treatment beam. J Radiat Res 2011;52:59–68.
[21] Kellerer AM, Rossi HH. The theory of dual radiation action. Curr Top Radiat Res 1972;8:85–158.
[22] ICRU, ICRU Report 36: Microdosimetry (1983).
[23] Loncol T, Cosgrove V, Denis JM, Gueulette J, Mazal A, et al. Radiobiological effectiveness of radiation beams with broad LET spectra: microdosimetric analysis using biological weighting functions. Rad Prot Dosim 1994;52:347–52.
[24] Cirrone GAP, Cuttone G, Di Rosa F, Raffaele L, Russo G, et al. The geant4 toolkit capability in the hadron therapy field: simulation of a transport beam line. Nucl Phys B 2005;150:54–7.
[25] Allison J, Amako K, Apostolakis J, Arce P, Asai M, et al. Recent developments in GEANT4. Nucl Instrum Meth A 2016;835:186–225.
[26] Romano F, Cirrone GAP, Cuttone G, Di Rosa F, Mazzaglia SE, Petrovic I, Ristic Fira A, Varisano A. A Monte Carlo study for the calculation of the average linear energy transfer (LET) distributions for a clinical proton beam line and a radiobiological carbon ion beam line. Phys Med Biol 2014;59:2863–82.
[27] Petringa G, Cirrone GAP, et al. Development and analysis of the track-LET, dose-LET and RBE calculations with a therapeutical proton and ion beams using Geant4 Monte Carlo code. Physica Medica 2017;42(1):9. https://doi.org/10.1016/j.ejmp.2017.09.023.
[28] Cirrone GAP, et al. Clinical and research activities at the CATANA Facility of INFN-LNS: from the conventional hadrontherapy to the laser-driven approach. Front. Oncol. 2017. https://doi.org/10.3389/fonc.2017.00223.
[29] GUM, Guide to the expression of uncertainty in measurement, JCGM 100; 2008.
[30] Pihet P, Menzel HG, Schmidt R, Beauduin M, Wambersie A. Biological weighting function for RBE specification of neutron therapy beams. Intercomparison of 9 European centres. Rad. Prot. Dosim. 1990;31(1-4):437–42.
[31] Gueulette J, et al. Intestinal crypt regeneration in mice: A biological system for quality assurance in non-conventional radiation therapy. Radiother Oncol 2005;73(Suppl 2):S148–54.
[32] Friedrich T, Scholz U, Elsässer T, Durante M, Scholz M. Systematic analysis of RBE and related quantities using a database of cell survival experiments with ion beam irradiation. J Radiat Res 2013;54(3):494–514.